https://doi.org/10.1007/s41230-022-1094-2

Effects of Zr additions on structure and tensile properties of an Al-4.5Cu-0.3Mg-0.05Ti (wt.%) alloy

***Hamed Kamali[1], Erfan Kamali[2], and Massoud Emamy[1]**

1. School of Metallurgy and Materials Engineering, College of Engineering, University of Tehran, P.O. Box 11155-4563, Tehran, Iran

2. Faculty of Materials Engineering, Sahand University of Technology, P.O. Box 51335-1996, Tabriz, Iran

Abstract: The effects of different Zr additions (0.05wt.%–0.5wt.%) on the structure and tensile properties of an Al-4.5Cu-0.3Mg-0.05Ti (wt.%) alloy solidified under a high cooling rate (18 °C·s^{-1}), in as-cast and T6 heat-treated conditions were studied. The as-cast structure of the alloy consists of equiaxed grains of α-Al with an average size of 64 μm which is unaffected by the Zr additions, indicating the ineffectiveness of Zr in the grain refinement of the alloy. Scanning electron microscopy, along with X-ray diffraction analysis revealed the presence of elongated θ-Al_2Cu at the grain boundaries; in addition, coarse Al_3Zr particles exist in the intergranular regions of the 0.5wt.% Zr-containing alloy. After the T6 heat treatment, the elongated θ particles were fragmented; however, the coarse Al_3Zr particles remained unchanged in the microstructure. Also, the formation of fine β'-Al_3Zr and θ''-Al_3Cu/θ'-Al_2Cu phases during T6 heat treatment was revealed by transmission electron microscopy. The results of the tensile tests showed that the Zr additions increase the strength of the alloy in both as-cast and T6 heat-treated conditions, but reduce its elongation, especially with 0.5wt.% Zr addition. The 0.3wt.% Zr-added alloy in the T6 heat-treated condition has the highest quality index value (249 MPa). Fractography of the fracture surfaces of the alloys revealed ductile fracture mode including dimples and cracked intermetallic phases in both conditions.

Keywords: Al-Cu-Mg alloys; casting; T6 heat treatment; structure; precipitation hardening; tensile properties; fractography

CLC numbers: TG146.21 **Document code:** A **Article ID:** 1672-6421(2022)01-009-08

1 Introduction

Al-Cu-Mg alloys have widespread applications in the aerospace and transportation industries, due to their high specific strength [1], good oxidation and corrosion resistance, high melting temperature (among Al alloys), and good thermal conductivity [2]. The excellent strength properties of these age-hardenable Al alloys originate from precipitation of the nanoscale metastable phases [1,3,4], namely θ''-Al_3Cu with a tetragonal structure (a=0.404 nm and c=0.768 nm), θ'-Al_2Cu with a tetragonal structure (a=0.404 nm and c=0.580 nm) [3,5,6], GPB2/S''-$Al_{10}Cu_3Mg_3$ with an orthorhombic structure (a=0.405 nm, b=1.620 nm and c=0.405 nm) [5,7], and S'-Al_2CuMg with an orthorhombic structure (a=0.405 nm, b=0.916 nm and c=0.720 nm) [1,5,6], in α-Al matrix during age hardening treatments.

***Hamed Kamali**

Male, born in 1987, Ph.D. His research interests mainly focus on processing-structure-property relationships in materials. He is also interested in conventional and high-resolution S/TEM.

E-mail: hamedkamali9974@gmail.com

Received: 2021-05-05; Accepted: 2021-12-04

However, Al-Cu-Mg alloys are extremely susceptible to hot tearing, due to their long solidification ranges [8,9], leading to a fracture as a result of strain localization in the solidifying alloy above its non-equilibrium solidus temperature [10,11]. The grain refinement of the as-cast structure using inoculation of grain refiners in the molten alloy is an approach to avoiding the formation of the hot tearing in Al-Cu-Mg alloys [10-12]. It has been shown that the addition of at least 0.05wt.% Ti as an Al-5Ti-1B (wt.%) grain refiner to an Al-4.5Cu-0.3Mg (wt.%) alloy (all compositions are in wt.% herein, unless otherwise specified) is necessary to prevent hot tearing [13].

The grain refining effect of Zr on commercial Al alloys has previously been reported [11,14-16]. Moreover, small Zr additions form fine spherical metastable coherent $L1_2$ β'-Al_3Zr dispersoids (typically 20–30 nm in diameter) during thermomechanical processing of Al alloys, inhibiting recrystallization and grain growth [6,16-18]. It is noted that the Zr contents of commercial Al alloys are usually limited to lower than 0.16% to avoid the formation of coarse primary Al_3Zr phase in the alloy melt during solidification under typical cooling rates [16]. Although it is expected that

solidification under high cooling rates may prevent the formation of the coarse primary Al_3Zr phase in commercial Al alloys, effects of higher Zr concentrations on the structure and tensile properties of Al-Cu-Mg alloys solidified under high cooling rates have not been investigated yet.

The present study aims to investigate the influences of different Zr additions (0.05%, 0.1%, 0.3%, and 0.5%) on the structure and tensile properties of an Al-4.5Cu-0.3Mg-0.05Ti alloy solidified under a high cooling rate (18 °C·s^{-1}), in as-cast and T6 heat-treated conditions to determine the optimum Zr content of the alloy in terms of the quality index parameter.

2 Experimental procedure

Commercially pure elemental Al and Mg, and Cu-50Al and Al-5Ti-1B master alloys were used to prepare an Al-4.5Cu-0.3Mg-0.05Ti alloy. All materials were melted in a resistance furnace using a silicon carbide (SiC) crucible (with 10 kg capacity for cast-iron melt) at 750 °C, and were poured into an open steel mold after gently hand stirring the melt with a graphite rod, and cleaning off the dross. The composition of the cast alloy is provided in Table 1.

Table 1: Composition of alloy studied (wt.%)

Cu	Mg	Fe	Ti	Si	Mn	Zn	B	Al
4.48	0.32	0.16	0.05	0.03	0.02	0.01	0.01	Bal.

Then, the ingot of the Al-4.5Cu-0.3Mg-0.05Ti alloy was cut into smaller pieces; and each piece was remelted in another resistance furnace using an SiC crucible (with 3 kg capacity for cast-iron melt) at 750 °C. After cleaning off the dross, the melt was further alloyed with desired amounts of an Al-5Zr master alloy to provide different Zr contents (0.05%, 0.1%, 0.3%, and 0.5%) in the castings. To ensure complete mixing, the molten alloy was stirred with a graphite rod for about 1 min. Then, degassing was conducted using C_2Cl_6 tablets (0.3% of the molten alloy) for about 2 min. After stirring and cleaning off the dross, the molten alloy was poured into a ductile iron mold [Fig. 1(a)] pre-heated to 150 °C to produce sub-sized tensile test samples according to ASTM B108/B108M-12e1 standard [Fig. 1(b)]. The cooling rates of the tensile samples during solidification were measured as ~18 °C·s^{-1} using a K-type thermocouple inserted into the middle of the gauge length parts of the samples [Fig. 1(a)]. The actual Zr contents of the samples with 0.05%, 0.1%, 0.3%, and 0.5% Zr additions were measured using a Spectrolab analyzer, as 0.049%, 0.098%, 0.283%, and 0.455%, respectively. To conduct T6 heat treatment, the tensile samples were solutionized at 530 °C for 12 h followed by water quenching to room temperature, and then were immediately aged at 160 °C for 12 h before air cooling [19]. The structural studies were carried out on the thin-section samples (6 mm diameter) cut from the gauge length parts of the tensile test castings [Fig. 1(b)]. The cut sections were polished using standard metallographic techniques, and then were etched using Keller's reagent (2 mL HF, 3 mL HCl, 5 mL HNO_3, and 190 mL H_2O) to reveal the structures. An optical microscope (OM) equipped with an image analysis system (Clemex Vision Pro. Ver. 3.5.025) was used to measure the average grain sizes of the samples, according to the linear intercept method (ASTM E112-12 standard).

Further microstructural characterization of the specimens was conducted on a CamScan MV2300 scanning electron microscope (SEM) operated at 25 kV, and equipped with an energy-dispersive X-ray spectroscopy (EDS) detector. Transmission electron microscopy (TEM) samples were prepared by twin-jet electropolishing in a 25vol.% nitric acid in methanol solution at

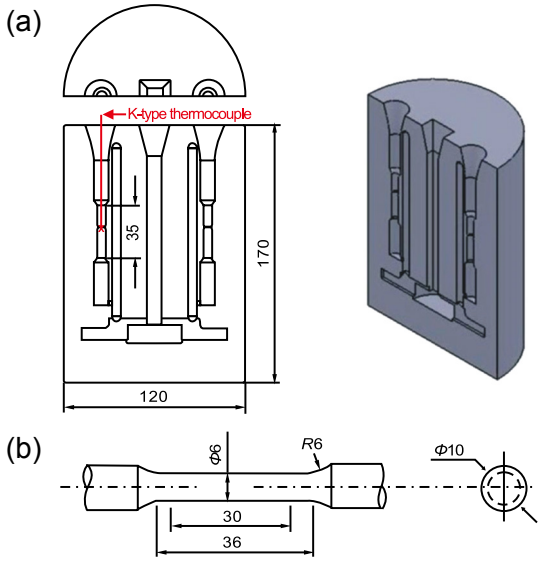

Fig. 1: Cast iron mold and position of thermocouple used for cooling rate measurements (a), and tensile test sample dimensions (b) (unit: mm)

−30 °C and 10−12 V. TEM was performed using an FEI Tecnai G^2 F20 TEM operated at 200 kV. Also, X-ray diffraction (XRD) analysis was conducted on a Philips X'pert Pro diffractometer using Cu Kα radiation. The hardness measurements of the samples were carried out in an ESEWAY universal hardness tester using a 30 kg load and a 2.5 mm diameter ball. At least seven measurements were performed at random positions on the surface of each specimen. The tensile tests were conducted on a computerized MTS tension machine equipped with a strain gauge extensometer at a constant cross-head speed of 1 mm·min^{-1} at room temperature. The fracture surfaces of the tensile samples were also characterized using the same SEM.

3 Results and discussion

3.1 Structural characterization

The OM as-cast microstructures of the Al-4.5Cu-0.3Mg-0.05Ti

alloy with the additions of different amounts of Zr consist of equiaxed grains and an elongated phase at the grain boundaries, as shown in Fig. 2. In addition, a coarse particle exists in the intergranular region of the 0.5% Zr-added sample [Fig. 2(e)].

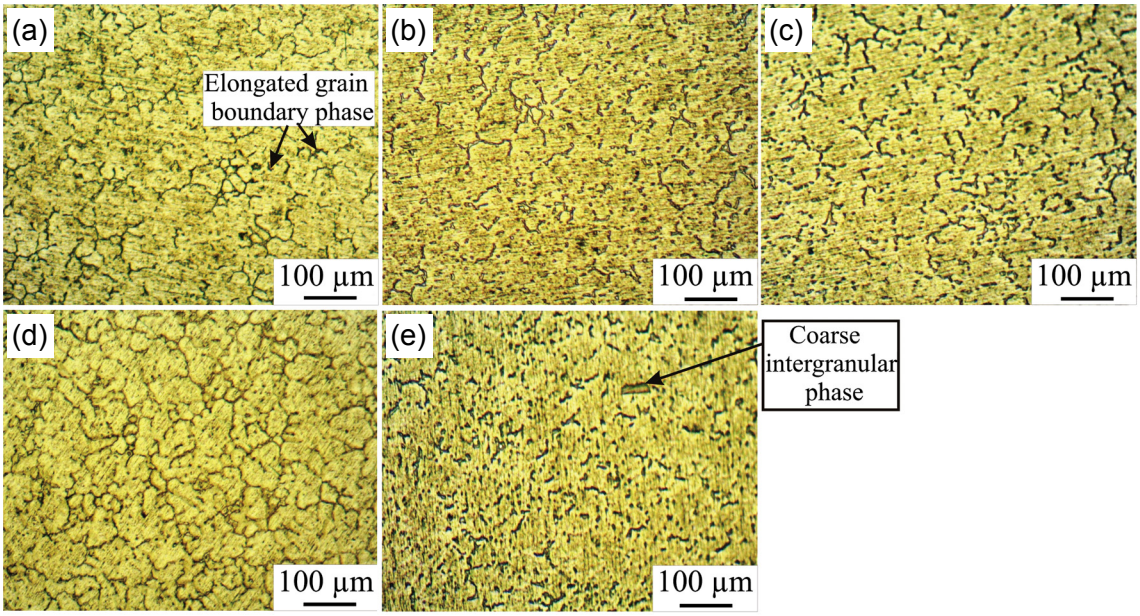

Fig. 2: OM as-cast microstructures of Al-4.5Cu-0.3Mg-0.05Ti alloy without (a) and with 0.05% (b), 0.1% (c), 0.3% (d), and 0.5% (e) Zr additions

The average grain sizes of the samples are summarized in Table 2, showing no significant change in the grain size of the Al-4.5Cu-0.3Mg-0.05Ti alloy by alloying with Zr up to 0.5%. This fact reveals the ineffectiveness of the Zr additions in the grain refinement of the Al-4.5Cu-0.3Mg-0.05Ti alloy solidified under 18 °C·s^{-1} cooling rate. A previous study [13] showed that the additions of more than 0.05% Ti to the Al-4.5Cu-0.3Mg alloy also have no obvious grain refining effects. These results indicate the saturation of the number density of the active heterogeneous nucleation sites [20] in the alloy containing 0.05% Ti during solidification under 18 °C·s^{-1} cooling rate. Also, the fact that Zr is a much less effective grain refiner than Ti for Al alloys [14,15], could be another reason for this observation.

Table 2: Average grain sizes of samples with different Zr contents

Zr content (wt.%)	Grain size (μm)	Std. dev. (μm)
0	64	8
0.05	65	7
0.1	63	8
0.3	61	7
0.5	63	8

XRD patterns taken from the Zr-free and 0.5% Zr-added samples in the as-cast condition are shown in Fig. 3. As can be seen, the diffraction peaks of the α-Al as the matrix, and θ-Al_2Cu as the elongated grain boundary phase (Fig. 2), are identified in both samples.

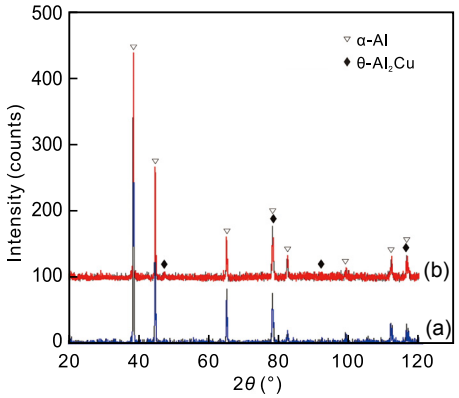

Fig. 3: XRD patterns of as-cast Zr-free (a) and 0.5% Zr-added (b) samples

Figure 4 illustrates the SEM microstructures of the as-cast Al-4.5Cu-0.3Mg-0.05Ti alloy with 0%, 0.05%, 0.1%, 0.3%, and 0.5% Zr additions. The α-Al grains and the elongated grain boundary θ-Al_2Cu phase are found with dark (lower atomic number) and bright (higher atomic number) contrasts, respectively, which the latter formed as a result of the eutectic reaction during the last stage of non-equilibrium solidification. It is noted that there are no coarse primary Al_3Zr particles in the as-cast microstructure of the 0.3% Zr-added alloy [Fig. 4(d)], since 0.3% Zr is soluble in the alloy melt at 750 °C [21], and the high cooling rate of the mold prevents the formation of the coarse primary Al_3Zr particles during subsequent cooling. However, the OM [Fig. 2(e)] and SEM [Fig. 4(e)] microstructures of the as-cast alloy containing 0.5% Zr, along with the SEM-EDS analysis in Fig. 4(e) reveal the existence of the coarse primary Al_3Zr particles in the intergranular regions.

These Al_3Zr particles formed in the alloy melt, since 0.5% Zr could not completely dissolve in the liquid Al at 750 °C [21]; and were subsequently pushed into the intergranular regions by the growing solid phase (α-Al) during solidification. It is noted that the diffraction peaks of the coarse Al_3Zr phase were not identified in the XRD pattern of the 0.5% Zr-containing sample [Fig. 3(b)] due to its too low volume fraction in the microstructure [Figs. 2(e) and 4(e)].

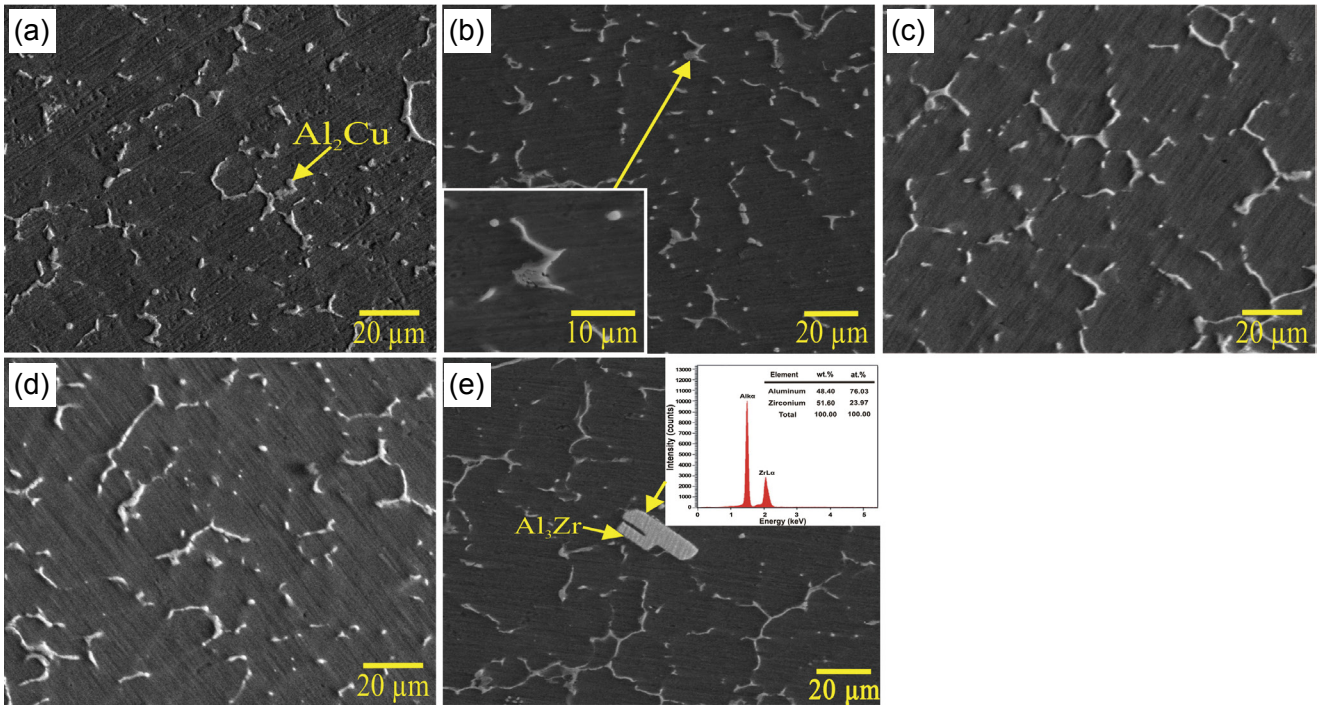

Fig. 4: SEM microstructures of as-cast Al-4.5Cu-0.3Mg-0.05Ti alloy with different Zr contents: (a) 0%, (b) 0.05%, (c) 0.1%, (d) 0.3%, and (e) 0.5%. The inset in (e) shows EDS point spectrum of Al_3Zr particle

The SEM microstructures of the Al-4.5Cu-0.3Mg-0.05Ti alloy with 0.05%, 0.1%, 0.3%, and 0.5% Zr additions after the T6 heat treatment are shown in Fig. 5. As can be observed, the elongated θ phase at the grain boundaries was partly dissolved and fragmented into smaller grain boundary precipitates during solution stage of the T6 heat treatment (530 °C for 12 h). Furthermore, the coarse Al_3Zr phase remained undissolved in the matrix [Fig. 5(d)] during solution treatment, as expected.

The bright-field TEM image in Fig. 6 shows the formation of the fine spherical β'-Al_3Zr dispersoids [6,17,18,22] along with the fine plate-like θ''-Al_3Cu/θ'-Al_2Cu precipitates [23,24] in the microstructure of the 0.3% Zr-added alloy after the T6 heat

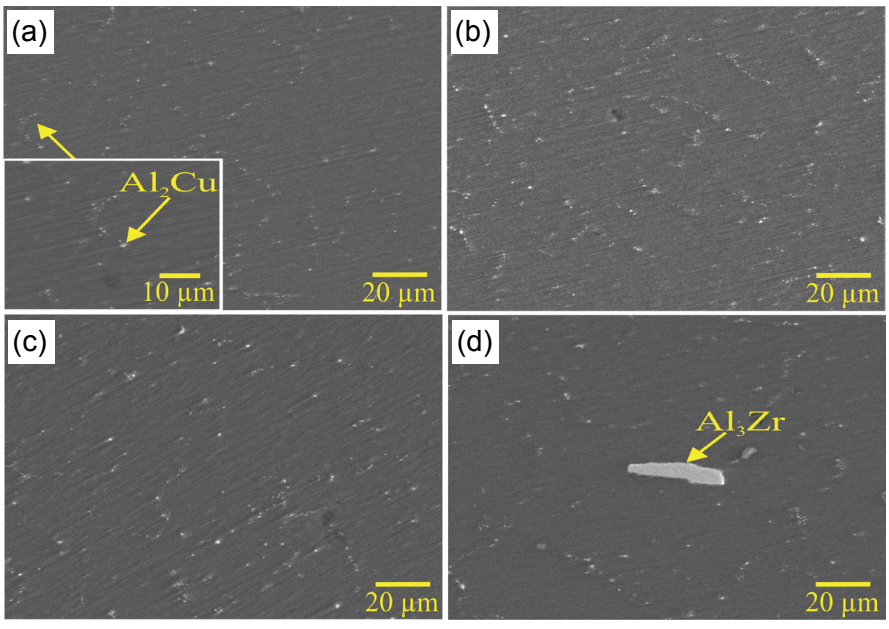

Fig. 5: SEM microstructures of T6 heat-treated Al-4.5Cu-0.3Mg-0.05Ti alloy with different Zr additions: (a) 0.05%, (b) 0.1%, (c) 0.3%, and (d) 0.5%

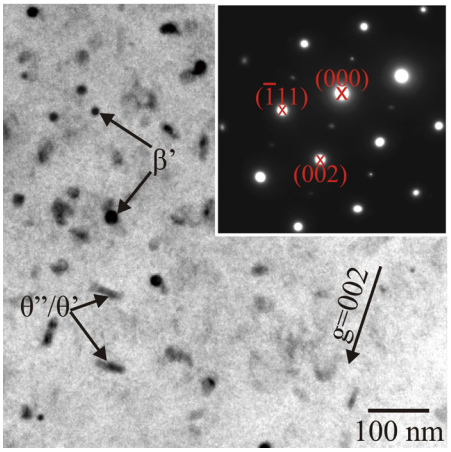

Fig. 6: Bright-field TEM image of 0.3% Zr-containing sample after T6 heat treatment taken near [110] zone axis. The inset shows corresponding [110] SADPs taken from β'-Al_3Zr dispersoids and matrix

treatment. The corresponding selected area diffraction patterns (SADPs) taken from the β' dispersoids and the α matrix (inset in Fig. 6) are consistent with the diffraction patterns along the [110] zone axis of both phases. It is further noted that the weak superlattice reflections in the SADP of the β' phase are in agreement with its $L1_2$ structure. Also, the orientation relationship between the β' dispersoids and the α matrix is consistent with the cube-on-cube orientation relationship (inset in Fig. 6).

3.2 Hardness, tensile properties and quality index evaluations

The yield strength at 0.2% offset (YS), and ultimate tensile strength (UTS), and Brinell hardness values of the samples with different Zr contents in the as-cast and T6 heat-treated conditions are shown in Figs. 7(a) and (b), and Table 3, respectively. As can be seen, the YS, UTS, and hardness values of the Zr-free alloy are gradually increased by alloying with Zr in the as-cast condition. This is mainly due to the solid solution strengthening effect of the supersaturated Zr atoms in the α-Al at room temperature, as a result of the approximate insolubility of Zr in the α-Al below 300 °C [21], and the high cooling rate of the tensile samples in the mold, along with sluggish precipitation kinetics of the β'-Al_3Zr phase in the α-Al matrix [17]. After the T6 heat treatment, the YS, UTS, and hardness values of the samples with different Zr additions are increased significantly [Figs. 7(a) and (b), Table 3], as a result of the dissolution of the elongated θ phase at the grain boundaries (Fig. 5) during solution at 530 °C for 12 h, and subsequently, precipitation of the nanoscale metastable θ''/θ' phases in the α-Al matrix (Fig. 6) [3,23,24] during aging at 160 °C for 12 h. Similar to the as-cast samples, increasing the Zr content of the alloy in the T6 heat-treated condition leads to a gradual increase in its hardness and strength values [Table 3, and Figs. 7(a) and (b)], due to precipitation of the nanoscale metastable β' dispersoids in the α-Al matrix (Fig. 6) [6,16-18,22]. Also, the non-shearable coarse primary Al_3Zr particles in the microstructure of the 0.5% Zr-added sample with a low volume fraction [Figs. 2(e), 4(e) and 5(d)], could slightly increase the hardness and YS values of the alloy in both as-cast and T6 heat-treated conditions, due to their blocking effect on movement of dislocations (Orowan mechanism) [18,22].

The elongation values of the Al-4.5Cu-0.3Mg-0.05Ti alloy in the as-cast and T6 heat-treated conditions are gradually decreased by alloying with Zr [Fig. 7(c)] as a result of the strengthening effects of the Zr additions. The elongation drops from 0.3% Zr to 0.5% Zr additions are more noticeable due to the existence of the coarse Al_3Zr particles in the microstructures of the 0.5% Zr-added samples [Figs. 2(e), 4(e) and 5(d)], which act as crack initiation sites [25]. Interestingly, the elongation values of the samples containing various amounts of Zr in the as-cast condition are tremendously increased by the T6 heat treatment, as a result of the dissolution of the elongated grain boundary θ phase (Fig. 5) which is responsible for the initiation of cracks in the as-cast microstructures (Figs. 2 and 4) [25].

To assess the quality of Al alloys, the quality index (Q) parameter, combining the strength and elongation values, has been introduced. Din et al. [26] proposed the following equation to calculate the Q parameter for Al-Cu alloys in the underaged conditions:

$$Q = \mathrm{YS} + KE \quad (1)$$

where E denotes elongation, and K is a material-dependent constant with a value of 7.5 MPa for A206-type Al-Cu-Mg alloys [26,27].

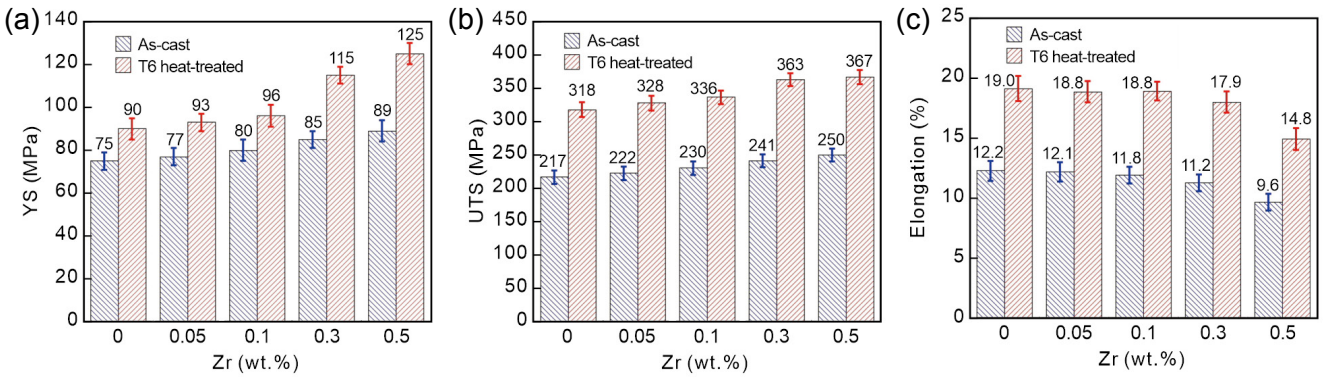

Fig. 7: YS (a), UTS (b), and elongation (c) values of Al-4.5Cu-0.3Mg-0.05Ti alloy versus its Zr content. The numbers on columns show average value of each column

The Q values of the samples were calculated using Eq. (1), as provided in Table 3. It can be seen the Q values of the samples containing different Zr contents increase significantly after the T6 heat treatment, due to the increases in both YS and elongation values [Figs. 7(a) and (c)]; and the 0.3% Zr-added alloy in the T6 heat-treated condition has the highest Q value (249 MPa), which is important from an industrial applications standpoint.

3.3 Fractography

Figure 8 shows the fracture surfaces of the 0.05% Zr-added samples in the as-cast and T6 heat-treated conditions. The occurrence of the necking in the fracture surface of the T6 heat-treated specimen indicates its higher deformation than the as-cast specimen, consistent with the higher elongation values of the samples after the T6 heat treatment [Fig. 7(c)].

Table 3: Mechanical properties of Al-4.5Cu-0.3Mg-0.05Ti alloy with different Zr additions in as-cast and T6 heat-treated conditions

Zr addition amount (wt.%)	State	Hardness (BHN)	Q (MPa)
0	As-cast	50	166
0.05		52	168
0.1		53	168
0.3		55	169
0.5		57	161
0	Heat-treated	85	232
0.05		87	234
0.1		88	237
0.3		93	249
0.5		94	236

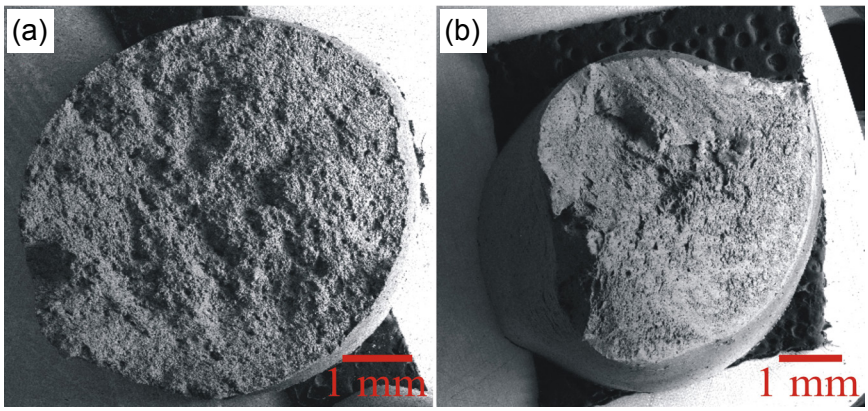

Fig. 8: Low magnification SEM images of fracture surfaces of Al-4.5Cu-0.3Mg-0.05Ti alloy containing 0.05% Zr in as-cast (a) and T6 heat-treated conditions (b)

Figures 9 and 10 exhibit the fracture surfaces of the Al-4.5Cu-0.3Mg-0.05Ti alloy with additions of 0.05%, 0.1%, 0.3%, and 0.5% Zr in the as-cast and T6 heat-treated conditions, respectively. The fracture surfaces predominantly illustrate ductile fracture mode including dimples and cracked θ particles (higher magnification insets of Figs. 9 and 10) in both conditions; however, the dimples are finer in the T6 heat-treated samples, consistent with the higher elongation values of the samples after the T6 heat treatment [Fig. 7(c)]. It is noted that the coarse θ phase (coarse intermetallic compound) along the grain boundaries in the microstructures of the samples in the as-cast condition (Figs. 2 and 4) is more prone to cracking at lower stresses and strains than the fine θ and metastable phases (fine intermetallic compounds) in the microstructures of the T6 heat-treated samples (Figs. 5 and 6), forming larger voids (corresponding to the larger dimples) [28]. Since the voids grow during further deformation until their coalescence (formation of void sheets) and beginning of the fracture [28], the formation of the larger voids results in the lower elongation of the samples. Figure 9(d) shows a cracked coarse Al_3Zr particle on the fracture surface of the 0.5% Zr-added alloy, along with microporosity adjacent to the particle, indicating the blocking

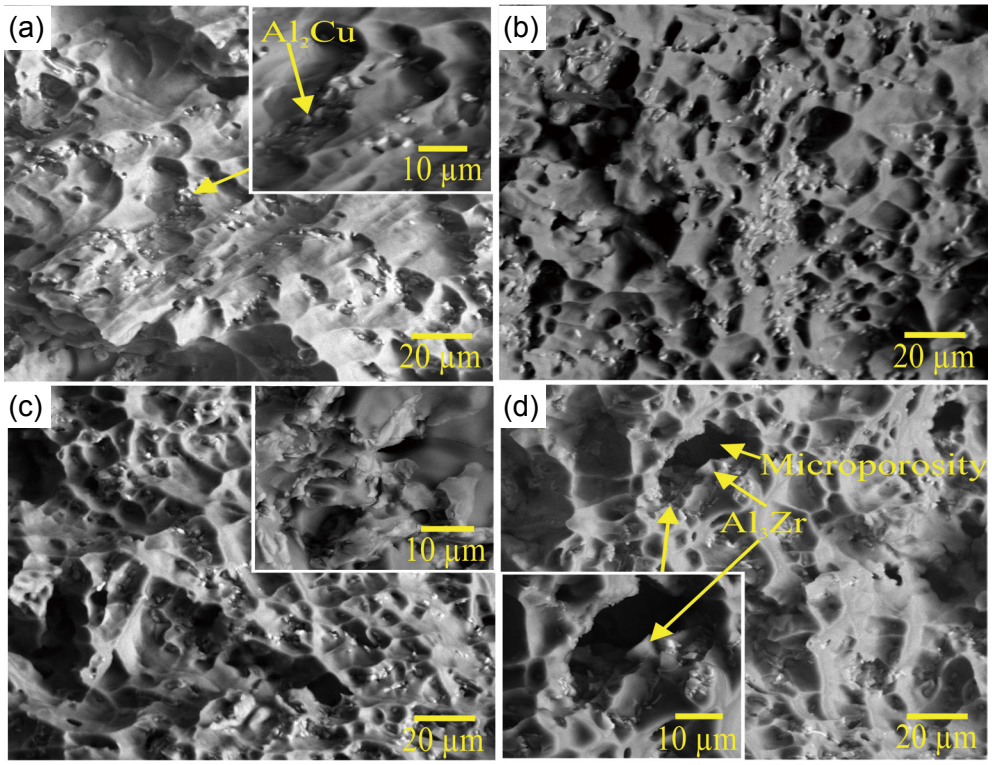

Fig. 9: High magnification SEM microstructures of fracture surfaces of Al-4.5Cu-0.3Mg-0.05Ti alloy with additions of 0.05% (a), 0.1% (b), 0.3% (c), and 0.5% (d) Zr in as-cast condition

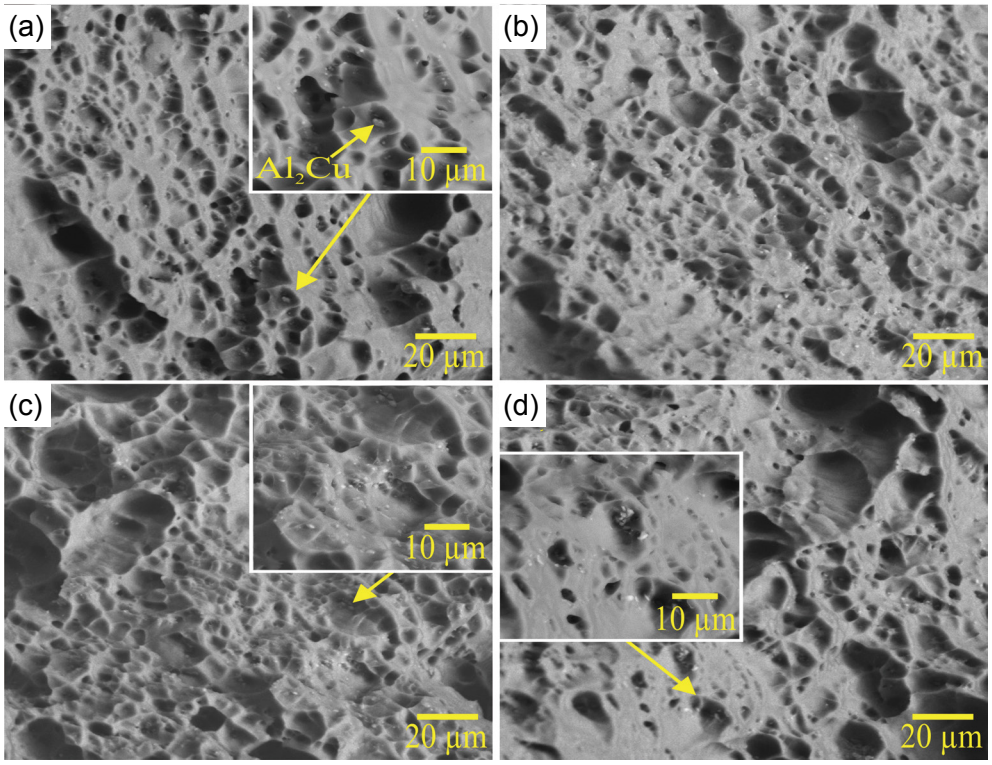

Fig. 10: High magnification SEM microstructures of fracture surfaces of Al-4.5Cu-0.3Mg-0.05Ti alloy containing 0.05% (a), 0.1% (b), 0.3% (c), and 0.5% (d) Zr in T6 heat-treated condition

effect of the coarse Al_3Zr on the liquid feeding in the last stages of solidification. Thus, the formation of the coarse Al_3Zr particles in the intergranular regions of the 0.5% Zr-containing alloy [Figs. 2(e), 4(e) and 5(d)], would have deleterious effects on the elongation [Fig. 7(c)].

4 Conclusions

Based on the structural characterization and tensile tests conducted on the Al-4.5Cu-0.3Mg-0.05Ti alloy with different Zr additions, solidified under the high cooling rate (18 °C·s^{-1}), in the

as-cast and T6 heat-treated conditions, the following conclusions can be drawn:

(1) The as-cast structure of the Al-4.5Cu-0.5Mg-0.05Ti alloy consists of the equiaxed grains of the α-Al with the average size of 64 μm. The grain size is not noticeably changed by alloying with Zr up to 0.5%, indicating the ineffectiveness of Zr in the grain refinement of the alloy. Also, the elongated θ phase exists at the grain boundaries in the as-cast microstructures of the samples. In addition, the coarse Al_3Zr particles are present in the intergranular regions of the as-cast 0.5% Zr-added sample, due to the incomplete dissolution of 0.5% Zr in the alloy melt at 750 °C.

(2) After the T6 heat treatment, the elongated θ phase at the grain boundaries is fragmented into smaller particles as a result of its dissolution in the α matrix during solution step; however, the coarse Al_3Zr particles remain unchanged in the microstructure of the 0.5% Zr-containing alloy. Also, the fine β' dispersoids and the fine θ''/θ' precipitates form in the microstructures during T6 heat treatment.

(3) The elongation values of the alloy gradually decrease while the hardness, YS, and UTS values gradually increase with the increase of the Zr addition amount in the as-cast and T6 heat-treated conditions. However, 0.5% Zr addition leads to significant drops in the elongation values of the alloy in both conditions, due to the existence of the coarse Al_3Zr particles in the microstructure.

(4) Both strength and elongation values of the samples are increased by the T6 heat treatment, leading to significant improvements in the quality index (Q) values of the samples. The T6 heat-treated alloy with 0.3% Zr has the highest Q value (249 MPa).

(5) The fracture surfaces of the samples with different Zr additions exhibit ductile fracture mode including the dimples and cracked intermetallic phases in the as-cast and T6 heat-treated conditions; the sizes of the dimples are finer in the T6 heat-treated samples, due to their finer θ, and nanoscale metastable phases.

Acknowledgement

The University of Tehran is acknowledged for providing lab facilities for this work.

References

[1] Polmear I J, StJohn D, Nie J F, et al. Light alloys: Metallurgy of the light metals. 5th edition, Arnold, London, 1995: 45–75, 284.
[2] Plevachuk Y, Sklyarchuk V, Yakymovych A, et al. Density, viscosity, and electrical conductivity of hypoeutectic Al-Cu liquid alloys. Metall. Mater. Trans. A, 2008, 39A: 3040–3045.
[3] Porter D A, and Esterling K E. Phase transformations in metals and alloys. 2nd edition, Chapman and Hall, London, 1992: 291–308.
[4] Kovarik L, Court S A, Fraser H L, et al. GPB zones and composite GPB/GPBII zones in Al-Cu-Mg alloys. Acta Mater., 2008, 56: 4804–4815.
[5] Wang S C, and Starink M J. Precipitates and intermetallic phases in precipitation hardening Al-Cu-Mg-(Li) based alloys. Inter. Mater. Rev., 2005, 50(4): 1–23.
[6] Prasad K S, Prasad N E, and Gokhale A A. Microstructure and precipitate characteristics of aluminum-lithium alloys. In: N. E. Prasad, A. A. Gokhale, and R. J. H. Wanhill (Eds.), Aluminum-lithium alloys: Processing, properties, and applications. Butterworth-Heinemann, Oxford, 2013: 99–137.
[7] Wang S C, and Starink M J. The assessment of GPB2/S" structures in Al-Cu-Mg alloys. Mater. Sci. Eng. A, 2004, 386: 156–163.
[8] Li Y Y, Guo G W, Zhang W W, et al. Effects of alloying elements on hot tearing trends of Al-Cu alloy. Trans. Nonferr. Met. Soc., 2001, 11: 765–791.
[9] Ganjehfard K, Taghiabadi R, Noghani M T, et al. Tensile properties and hot tearing susceptibility of cast Al-Cu alloys containing excess Fe and Si. Int. J. Miner. Metall. Mater., 2021, 28(4): 718–728.
[10] Kamga H K, Larouche D, Bournane M, et al. Hot tearing of aluminum-copper B206 alloys with iron and silicon additions. Mater. Sci. Eng. A, 2010, 527: 7413–7423.
[11] Li Y, Li H, Katgerman L, et al. Recent advances in hot tearing during casting of aluminium alloys. Prog. Mater. Sci., 2021, 117: 100741. https://doi.org/10.1016/j.pmatsci.2020.100741.
[12] Yoshida Y, Esaka H, and Shinozuka K. Effect of solidified structure on hot tear in Al-Cu alloy. IOP Conf. Ser.: Mater. Sci. Eng., 2015, 84: 1–6.
[13] Kamali H, Emamy M, and Razaghian A. The influence of Ti on the microstructure and tensile properties of cast Al-4.5Cu-0.3Mg alloy. Mater. Sci. Eng. A, 2014, 590: 161–167.
[14] Murty B S, Kori S A, and Chakraborty M. Grain refinement of aluminium and its alloys by heterogeneous nucleation and alloying. Inter. Mater. Rev., 2002, 47(1): 3–29.
[15] Guan R G, and Tie D. A review on grain refinement of aluminum alloys: Progresses, challenges and prospects. Acta Metall. Sin. (Engl. Lett.), 2017, 30(5): 409–432.
[16] He Y D, Zhang X M, and You J H. Effect of minor Sc and Zr on microstructure and mechanical properties of Al-Zn-Mg-Cu alloy. Trans. Nonferr. Met. Soc. China, 2006, 16: 1228–1235.
[17] Robson J D, and Prangnell P B. Dispersoid precipitation and process modelling in zirconium containing commercial aluminum alloys. Acta Mater., 2001, 49: 599–613.
[18] Mochugovskiy A G, Mikhaylovskaya A V, Zadorognyy M Y, et al. Effect of heat treatment on the grain size control, superplasticity, internal friction, and mechanical properties of zirconium-bearing aluminum-based alloy. J. Alloys Compd., 2021, 856: 157455. https://doi.org/10.1016/j.jallcom.2020.157455.
[19] Davis J R, ed. Heat treating. ASM Handbook, ASM International, Materials Park, Ohio, 1991: 849.
[20] Maxwell I, and Hellawell A. A simple model for grain refinement during solidification. Acta Metall., 1975, 23: 229–237.
[21] Murray J, Peruzzi A, and Abriata J P. The Al-Zr (aluminum-zirconium) system. J. Phase Equilib., 1992, 13(3): 277–291.
[22] Souza P H L, Oliveira de C A S, and Vale Quaresma do J M. Precipitation hardening in dilute Al-Zr alloys. J. Mater. Res. Technol., 2018, 7: 66–72.
[23] Chen Y, Zhang Z, Chen Z, et al. The enhanced theta-prime (θ') precipitation in an Al-Cu alloy with trace Au additions. Acta Mater., 2017, 125: 340–350.
[24] Bourgeois L, Zhang Y, Zhang Z, et al. Transforming solid-state precipitates via excess vacancies. Nature Commun., 2020, 11: 1248. https://doi.org/10.1038/s41467-020-15087-1.
[25] Song M, Chen K H, and Qi X W. Modeling effects of constituents and dispersoids on tensile ductility of aluminum alloy. Cent. South Univ. Technol., 2007, 14(4): 456–459.
[26] Din T, Rashid A K M B, and Campbell J. High strength aerospace casting alloys: Quality factor assessment. Mater. Sci. Technol., 1996, 12: 269–273.
[27] Ammar H R, Samuel A M, Samuel F H, et al. The concept of quality index and its application for Al-Si cast alloys. Inter. Metalcast., 2021, 15(4): 1197–1212. https://doi.org/10.1007/s40962-020-00556-6.
[28] Van Stone R H, and Psioda J A. Discussion of "Metallurgical factors affecting fracture toughness of aluminum alloys". Metall. Trans. A, 1975, 6: 668–670.